Short Papers

Gross Motion Analysis of Fingertip-Based Within-Hand Manipulation

Nicolas Rojas, *Member, IEEE*, and Aaron M. Dollar, *Senior Member, IEEE*

Abstract—Fingertip-based within-hand manipulation, also called precision manipulation, refers to the repositioning of a grasped object within the workspace of a multifingered robot hand without breaking or changing the contact type between each fingertip and the object. Given a robot hand architecture and a set of assumed contact models, this paper presents a method to perform a gross motion analysis of its precision manipulation capabilities, regardless of the particularities of the object being manipulated. In particular, the technique allows the composition of the displacement manifold of the grasped object relative to the palm of the robot hand to be determined as well as the displacements that can be controlled—useful for high-level design and classification of hand function. The effects of a fingertip contacting a body in this analysis are modeled as kinematic chains composed of passive and resistant revolute joints; what permits the introduction of a general framework for the definition and classification of nonfrictional and frictional contact types. Examples of the application of the proposed method in several architectures of multifingered hands with different contact assumptions are discussed; they illustrate how inappropriate contact conditions may lead to uncontrollable displacements of the grasped object.

Index Terms—Dexterous manipulation, kinematic manipulation, multifingered hands, within-hand manipulation.

I. Introduction

The purposeful movement of an object within a multifingered robot hand by the relative motion of its fingers is generally known as robotic dexterous manipulation [1], [2]. Despite the importance of this functionality for the successful deployment of robots in real-world tasks, and the recent progress in the area [3], [4], the development of mechanical systems that reliably perform autonomous dexterous manipulation outside controlled environments is still an open problem [5].

Much work remains to be done in both robot hand design and control to enable dexterous manipulation capabilities. In this paper, we present a technique useful for both of these domains. The method is based on the analysis of the capabilities of robot hands for performing dexterous manipulation; in particular, manipulation activities in which a grasped object is repositioned within the hand without breaking or changing contact. These kinds of tasks can be classified as within-hand prehensile manipulation with no motion at contact via the manipulation taxonomy presented in [1]. More specifically, we say herein that this type of

N. Rojas is with the Department of Engineering and Design, University of Sussex, Brighton BN1 9QT, U.K. (e-mail: n.rojas@sussex.ac.uk).

A. M. Dollar is with the Department of Mechanical Engineering and Materials Science, Yale University, New Haven, CT 06511 USA (e-mail: aaron.dollar@yale.edu).
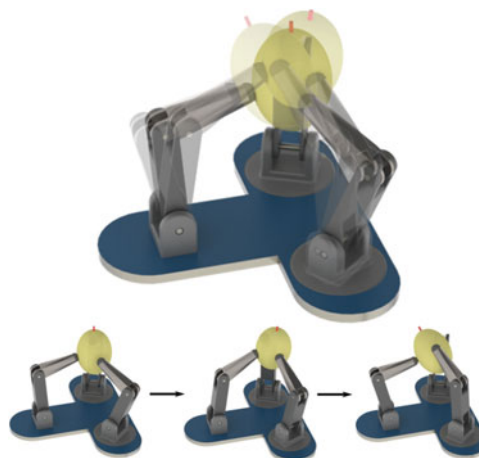
Fig. 1. In fingertip-based within-hand manipulation, or precision manipulation, a grasped object is repositioned within the hand workspace without breaking or changing the assumed contact model between each fingertip and the object.

dexterous manipulation task is performed without modifications in the assumed contact model between each fingertip and the object, and refer to it as precision manipulation (see Fig. 1) for the remainder of this paper (although the term has been used for a broader class of manipulation in other works [6], [7]).

The aim of the suggested approach is to characterize the precision manipulation capabilities of a given robot hand architecture by determining the feasible movements to reposition a grasped object within the hand workspace without breaking or changing the assumed contact models. In this analysis, the feasibility of motion refers to the composition of the displacement manifold of the object relative to the palm of the robot hand. The proposed characterization of manipulation ends by defining which of these possible displacements can actually be controlled by the hand actuators without depending on external factors (e.g., forces) to the hand.

Given that our interest is in general displacement characteristics (i.e., gross motion) regardless of the particularities of the grasped object and the infinitesimal (or local) motion features and limitations resulting from the dimensions of the fingers and the relation between the locations of the links composing them, we call this study: finite precision manipulation analysis. The proposed method is based on the Hervé's approach for the kinematics of mechanisms using the continuous group of displacements [8], a mathematical tool that has found its milestone application in the type synthesis of parallel platforms [9], [10]. Approaches based on screw theory could also be taken [11]; but special attention should be paid to identify the finite motion of the resulting instantaneous analysis, a step that could be difficult for some robot hand architectures. Table I presents a description of some of the subgroups of displacements—with their associated lower kinematic pair—that are relevant for our discussion. For a complete list of subgroups, see [12].

TABLE I
SUBGROUPS OF DISPLACEMENTS

Subgroup	Lower kinematic pair	Description
$\{\mathbf{I}\}$		The identity displacement. Rigid connection between bodies, no relative motion (0 DOF)
$\{\mathbf{R}(N, u)\}$	Revolute joint	Rotation about the axis determined by the unit vector u and point N (1 DOF)
$\{\mathbf{T}(v)\}$	Prismatic joint	Translation parallel to the unit vector v (1 DOF)
$\{\mathbf{C}(N, u)\}$	Cylindrical joint	Cylindrical motion about the axis determined by the unit vector u and point N (2 DOF)
$\{\mathbf{P}(v)\}$		Planar translation on the plane determined by the unit normal vector v (2 DOF)
$\{\mathbf{S}(N)\}$	Spherical joint	Spherical rotation about a point N (3 DOF)
$\{\mathbf{G}(v)\}$	Planar joint	Planar gliding motion on the plane determined by the unit normal vector v (3 DOF)

A comprehensive list of nonidentity intersections between subgroups of displacements can be found in [11, Table C.3].

A preliminary version of the presented framework for manipulation characterization was introduced in [13], where it was limited to contacts modeled as point contact with friction. In this paper, we further extend that framework by modeling the effects of a fingertip contacting a body as kinematic chains using an extension of the Bruyninckx–Hunt approach of surface–surface contact [14], what allows using all standard contact categories of robotic manipulation (e.g., point contact with friction, soft finger) as well as other contact models, such as ball, tubular, and frictional adaptive finger contacts. Moreover, the proposed technique extends the standard notion of finite (gross) kinematic manipulation, which has been historically restricted to the mobility analysis of multifinger grasps [15]–[17]. The identification of the uncontrollable displacements of a grasped object as herein suggested is relevant for the implementation of robotic dexterous tasks because it naturally leads to modifications in the design of the robot hand under study (fingers, fingertips, and palm layout) or its control scheme in order to avoid the resulting undesirable circumstances. The computation of the composition of the displacement manifold of the grasped object using the proposed analysis is also significant to robot hand design and control as it can be used to incorporate explicit motions in the system to perform specific tasks.

The rest of this paper is organized as follows. Section II discusses some of the essential ideas and tools required for understanding the proposed kinematic manipulation method. Section III details the steps to perform the precision manipulation analysis of a given robot hand using, as reference to introduce the different stages, a simple two-fingered hand with revolute–revolute opposed fingers. Two additional examples of more complex fingertip-based in-hand manipulation analyses are detailed in Section IV, namely a three-fingered hand layout commonly found in commercial robot hands and a four-fingered hand with revolute–revolute–revolute fingers. We finally conclude in Section V.

II. BACKGROUND

A. Kinematic Chains and Mobility

A kinematic chain can be characterized by its structural factors: number L of links, number J of joints, and total number of degrees of freedom (DOF) F of the joints; the set of relations $\boldsymbol{\theta}$ between link locations; the set of relations $\boldsymbol{\alpha}$ between joint axes; and the set of dimensions $\mathbf{S}$ of the links. The essential property of a kinematic chain is its mobility, which can be defined as the minimum number of independent parameters to make a kinematic chain rigid. The mobility of a kinematic chain usually indicates the number of joints that have to be actuated to control a robot mechanism.

It is widely known that the total mobility of a kinematic chain, say M_T, is a function not only of the structural parameters L, J, and F but of the sets $\boldsymbol{\theta}$, $\boldsymbol{\alpha}$, and $\mathbf{S}$ [18] as well. The so-called overconstrained mechanisms, such as the Bennett spatial four-bar linkage or the Bricard spatial six-bar linkage, are the classical examples of this fact. Thus, in general

$$M_T (\mathrm{L, \ J, \ F}, \boldsymbol{\theta}, \ \boldsymbol{\alpha}, \mathbf{S}) \ \geq \ M (\mathrm{L, J, F})$$
$$M_T (\mathrm{L, \ J, \ F}, \boldsymbol{\theta}, \ \boldsymbol{\alpha}, \mathbf{S}) \ = \ M (\mathrm{L, J, F}) + \varepsilon (\boldsymbol{\alpha}, \boldsymbol{\theta}, \mathbf{S}) \quad (1)$$

where $M(\mathrm{L, J, F})$ corresponds to the structural mobility (or generic mobility) of the kinematic chain and $\varepsilon(\boldsymbol{\alpha}, \boldsymbol{\theta}, \mathbf{S})$ is the degree of mobility added to the system by the conditions on the sets $\boldsymbol{\theta}$, $\boldsymbol{\alpha}$, and $\mathbf{S}$.

The factor $\varepsilon(\boldsymbol{\alpha}, \boldsymbol{\theta}, \mathbf{S})$ in (1) can be divided into the contribution given by the geometry of the joint axes ($\boldsymbol{\alpha}$) and that given by the geometry of the links ($\boldsymbol{\theta}, \mathbf{S}$), that is, $\varepsilon(\boldsymbol{\alpha}, \boldsymbol{\theta}, \mathbf{S}) = \varepsilon_1(\boldsymbol{\alpha}) + \varepsilon_2(\boldsymbol{\theta}, \mathbf{S})$. Then, since $M(\mathrm{L, J, F}) + \varepsilon_1(\boldsymbol{\alpha})$ does not depend on the dimensions or locations of the links, it is called the finite mobility of the mechanism. Given that formulas for $\varepsilon_1(\boldsymbol{\alpha})$ and $\varepsilon_2(\boldsymbol{\theta}, \mathbf{S})$ are unknown, recursive processing methods or algorithms based on the rank of the Jacobian matrix at a given configuration are used for the computation of M_T instead [18]. However, it has been proven that if M is computed using the extended Chebychev–Kutzbach–Grübler criterion, it is unlikely that $M_T \neq M$ when a kinematic chain is selected at random [19]. According to this criterion, the generic mobility of a mechanism is

$$M = \mathrm{F} - \sum_{i=1}^{\lambda} t_i \quad (2)$$

where $\lambda = \mathrm{J} - \mathrm{L} + 1$ is the number of independent (fundamental) loops of the kinematic chain and t_i is the motion type of the ith independent loop ($t_i = 3$ in the planar and spherical case, and $t_i = 6$ in the spatial case), with $M = 0$ if $\mathrm{F} < \sum_{i=1}^{\lambda} t_i$.

B. Kinematic Equivalents of Contact Models

According to the notation of Fig. 2, given two bodies touching at a single point C with Φ_A and Φ_B being smooth surfaces representing their boundaries in the neighborhood of the contact point (i.e., Φ_A and Φ_B have the same tangent plane at C), let
1) A_r and A_R (correspondingly B_r and B_R) be the centers of maximum and minimum curvature of Φ_A (Φ_B), respectively,
2) $u_\mathbf{a}$ and $w_\mathbf{a}$ (correspondingly $u_\mathbf{b}$ and $w_\mathbf{b}$) be the directions of maximum and minimum curvature of Φ_A (Φ_B), respectively, and
3) v a unit normal vector defining the common contact tangent plane.

From elementary differential geometry, it is known that u_i, w_i, and $v(i = \mathbf{a}, \mathbf{b})$ are orthogonal with directions uniquely defined unless the surface is locally a sphere or a plane. For these particular cases, there exist an infinite number of directions for the vectors u and w.
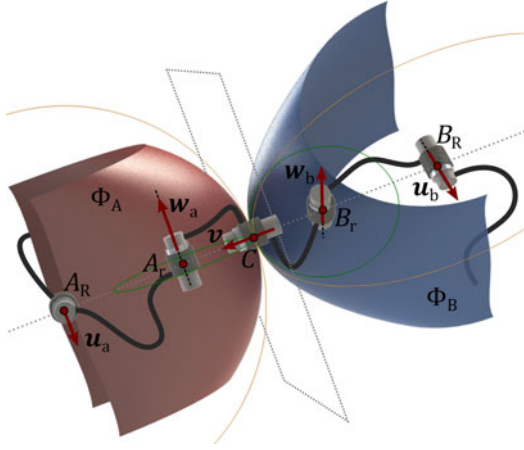
Fig. 2. Bruyninckx–Hunt model, a general kinematic-chain-based model of point contact without friction. The model consists of five serially connected passive revolute joints whose location and direction are unequivocal.
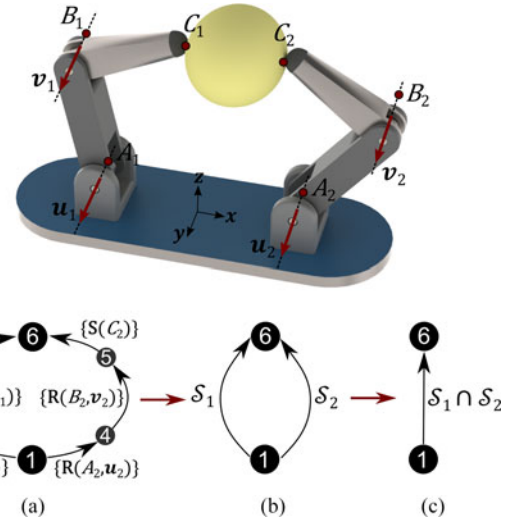

Fig. 3. Top: A 2F-2RR robot hand grasping an object with the notation used for its finite precision manipulation analysis with point contact with friction contacts. Bottom: The graph of kinematic constraints of the hand–object system for the 2F-2RR hand (a) and its corresponding reduction (b, c).

Fig. 2 corresponds to the generalized kinematic-chain-based model of point contact without friction, called herein the Bruyninckx–Hunt model. It consists of five serially connected passive revolute joints whose location and direction are unequivocal. The model is built by serially connecting revolute joints at points A_r, A_R, B_r, B_R, and C in the direction determined by vectors u_a, w_a, u_b, w_b, and v, respectively, and rigidly connecting the revolute joints at A_R and B_R to Φ_A and Φ_B. The resulting mechanism is a five-revolute chain of six links that provides five independent degrees of freedom of motion between the touching objects. By applying serial reduction to this kinematic chain, we get

$$\{\mathbf{R}\left(A_R, u_a\right)\} \cdot \{\mathbf{R}\left(A_r, w_a\right)\} \cdot \{\mathbf{R}\left(C, v\right)\}$$
$$\cdot \{\mathbf{R}\left(B_r, w_b\right)\} \cdot \{\mathbf{R}\left(B_R, u_b\right)\}. \qquad (3)$$

The above equation is the kinematic equivalent of the Bruyninckx–Hunt model. A kinematic equivalent simply corresponds to a single kinematic constraint (i.e., a subset of the continuous group of displacements) that represents the constrained motion between two contacting bodies.

Despite the explicit local definition of the Bruyninckx–Hunt model, useful novel finite kinematic equivalents of contact types can be defined since suppositions about the Gaussian curvature of the fingertip (and the object) can be made. Additionally, nonfrictional and frictional cases can be considered by replacing the three passive revolute joints of one of the surfaces (including the revolute joint at the contact point) by resistant passive joints; that is, passive joints able to resist moments till some value η before entering in motion.

A general classification of contact types for robot precision manipulation based on the above extended Bruyninckx–Hunt model was introduced in [14]. In such classification, all standard contact categories used in robotic manipulation, namely the Salisbury's taxonomy plus line–line contact without friction, appeared as special cases, and new contact models are defined and characterized via kinematic equivalents. Examples of these new contact models include ball, tubular, planar translation, and frictional adaptive finger contacts.

III. PRECISION MANIPULATION ANALYSIS

The objective of this study is, first, to define the feasible movements to reposition a grasped object within the hand workspace without break-

ing or changing the assumed contact model between each fingertip and the object, a task we refer to as precision manipulation and, second, to determine which of these possible displacements are controllable. By feasible movements, we mean the displacement manifold (finite motion) of the object relative to the base or palm of the robot hand. Controllable movements refer to the subset of these feasible displacements that can actually be controlled by the hand actuators.

The proposed approach is based on a group-theoretic analysis of the kinematic constraints associated with the hand–object system. We are interested in general displacement characteristics; the instantaneous (or local) motion features and limitations resulting from, for instance, the particular dimensions of the hand–object system or the friction conditions of the contacts, are not considered. The result of the method is a mathematical characterization of the finite within-hand manipulation capabilities of the hand regardless of the particularities of the grasped object. Next, we describe the five steps to perform such analysis for a given robot hand; the two-fingered hand with revolute–revolute opposed fingers (2F-2RR) of Fig. 3 will be used as a reference to introduce the different stages.

A. Initial Steps for the Analysis of Precision Manipulation

Fig. 3(top) shows a 2F-2RR hand grasping, with its fingertips, a general object—represented as an egg-shaped body in the image. This hand is composed of two identical fingers with two links (proximal and distal) arranged in an opposed configuration. In each finger, the proximal link is connected to the palm through a revolute joint, which determines the motion plane of the finger. The proximal and distal links are connected by another revolute joint whose axis is parallel to the proximal one. The motion plane of both fingers is parallel.

Given a robot hand composed of serial fingers, the first step to analyze its finite precision manipulation capabilities is to select a contact model, with its corresponding kinematic equivalent according to [14], for each of its fingertips. For the case of the 2F-2RR, we select the model of point contact with friction for the two fingertips, which corresponds to a limit instance of the elliptic contact model. The second step of the analysis is to determine the resulting kinematic chain of the hand–object system, given the robot hand topology and the assumed contact models for the
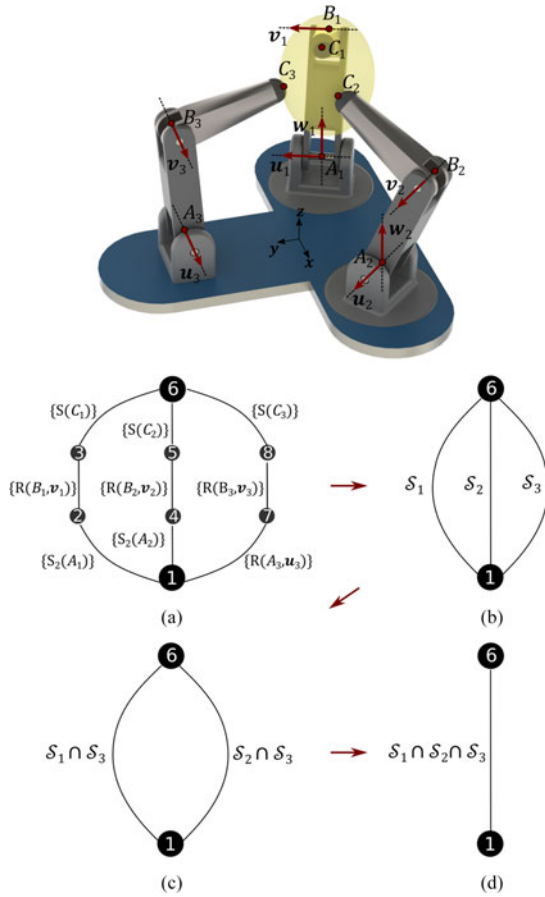
Fig. 4. Top: A 3F-2UR1R robot hand grasping an object with the notation used for its precision manipulation analysis with point contact with friction contacts. Bottom: The graph of kinematic constraints of the hand–object system for the 3F-2UR1R hand (a) and its corresponding reduction (b, c, d).

fingertips, and compute its corresponding structural mobility M using (2).

In our example, the hand–object system of the 2F-2RR hand with point contact with friction is equivalent to a closed kinematic chain composed of six links with two revolute–revolute–spherical serial limbs that connect the palm of the robot hand, or base, to the grasped object. The mobility of such closed kinematic chain (six links, six joints in $\mathbb{E}^3$ with a total number of 10 DOF in the joints) is 4. This implies that the feasible movements of a grasped object respect to the base correspond to a four-manifold (immersed in $\mathbb{E}^3$), in other words, the object has 4 DOF.

The third step in our analysis is to construct a graph of kinematic constraints of the resulting kinematic chain. For the case of our introductory example, according to the notation of Fig. 4(top), for the left finger, the axis of the ground revolute joint (or proximal joint) is determined by a unit vector u_1, that is parallel to the y-axis of the palm's reference frame ($u_1 \parallel y$), and any point, say A_1, that belongs to the line defined by the rotational axis. This kinematic pair corresponds to a kinematic constraint that forms the subgroup of displacements $\{\mathbf{R}(A_1, u_1)\} = \{\mathbf{R}(A_1, y)\}$ that restrict the movement between the proximal link and the palm. Similarly, for the case of the distal joint, the generated subgroup is $\{\mathbf{R}(B_1, v_1)\} = \{\mathbf{R}(B_1, y)\}$. Finally, assuming that the contact point between the fingertip and the object is C_1, the motion constraint between the two bodies under the supposition of point contact with friction generates the subgroup $\{\mathbf{S}(C_1)\}$.

By replicating this analysis in the right finger, we can construct the graph of kinematic constraints of this hand–object system as depicted in Fig. 3(bottom-a).

B. Reduction of the Graph of Kinematic Constraints

Given a robot hand (or subset of it) of n serial fingers grasping an object with all its fingertips; the resulting graph of kinematic constraints of the hand–object system, under the assumed contact models, has L nodes, J edges, and $\lambda = \mathrm{J} - \mathrm{L} + 1$ fundamental loops (cyclomatic number). For each of these loops, it is possible to compute its structural mobility using (2). The fourth step in the finite precision manipulation analysis is to reduce such graph to a single edge connecting the nodes associated with the robot's palm and the grasped object.

The above reduction process is carried out by first applying n operations of serial reductions (i.e., composition of the kinematic constraints involved in the nodes), one per each of the fingers in the hand–object system. Then, we get a graph of two nodes and n edges with λ fundamental loops. If λ operations of parallel reduction are applied to this graph (i.e., intersection of the kinematic constraints associated with two selected edges), we obtain a new graph of $n - 1$ edges and $\lambda - 1$ fundamental loops. Thus, systematically, after $\frac{\lambda(\lambda+1)}{2}$ operations of parallel reductions, we get a graph of two nodes and a single edge. In these operations is fundamental to take into account that variations in the expected structural mobility of each fundamental loop can appear from the factor $\varepsilon_1(\boldsymbol{\alpha})$ of the total mobility. Moreover, some parallel reductions can be avoided if all their involved edges have been already covered by other reductions. The final edge indeed corresponds to the kinematic constraint describing the composition of the displacement of the grasped object. The degrees of freedom of this last kinematic constraint should be equal to the structural mobility M computed in the second step unless that contributions from $\varepsilon_1(\boldsymbol{\alpha})$ have been detected in the reduction process of the graph.

In the case of the 2F-2RR hand with the model of point contact with friction, the original graph has six nodes, six edges, and $\lambda = 1$ fundamental loops. Then, first, using the notation of Fig. 3(bottom-a), we apply serial reduction to the nodes 1, 2, 3, and 6. Thus, we get

$$\mathcal{S}_1 = \{\mathbf{R}(A_1, y)\} \cdot \{\mathbf{R}(B_1, y)\} \cdot \{\mathbf{S}(C_1)\} \tag{4}$$

where $\mathcal{S}_1$ is a kinematic constraint defined as the subset of the group of rigid-body displacements resulting from the composition operation of the subgroups involved in the related nodes. Now, since the subgroup $\{\mathbf{R}(C_1, y)\}$ is a proper subset of the subgroup $\{\mathbf{S}(C_1)\}$, that is, $\{\mathbf{R}(C_1, y)\} \subset \{\mathbf{S}(C_1)\}$, then, by the property of closure, we get $\{\mathbf{R}(C_1, y)\} \cdot \{\mathbf{S}(C_1)\} = \{\mathbf{S}(C_1)\}$ $(\forall x, x \in \{\mathbf{R}(C_1, y)\} \cdot \{\mathbf{S}(C_1)\},\ x \in \{\mathbf{S}(C_1)\})$. Hence, $\mathcal{S}_1$ can be written as

$$\begin{aligned} \mathcal{S}_1 &= \{\mathbf{R}(A_1, y)\} \cdot \{\mathbf{R}(B_1, y)\} \cdot \{\mathbf{R}(C_1, y)\} \cdot \{\mathbf{S}(C_1)\} \\ &= \{\mathbf{G}(y)\} \cdot \{\mathbf{S}(C_1)\}. \end{aligned} \tag{5}$$

Applying the same serial reduction to the nodes 1, 4, 5, and 6, we get (with $u_2 \parallel v_2 \parallel y$)

$$\mathcal{S}_2 = \{\mathbf{G}(y)\} \cdot \{\mathbf{S}(C_2)\}. \tag{6}$$

Thus, after the application of the two serial reductions to the original graph of kinematic constraints, a reduced graph of two nodes with two edges is obtained, see Fig. 4(bottom-b). The nodes of such graph are the base (the palm of the robot hand) and the grasped object, both connected by the kinematic constraints $\mathcal{S}_1$ and $\mathcal{S}_2$.

Since $\lambda = 1$ in this particular example, a single parallel reduction operation applied to $\mathcal{S}_1$ and $\mathcal{S}_2$ is needed for reducing the graph to two

nodes and one edge [see Fig. 4(bottom-c)]. Then, we finally have

$$
\begin{aligned}
\mathcal{P}_1 &= \mathcal{S}_1 \cap \mathcal{S}_2 \\
&= \{\mathbf{G}\,(y)\} \cdot \{\mathbf{S}\,(C_1)\} \cap \{\mathbf{G}\,(y)\} \cdot \{\mathbf{S}\,(C_2)\} \\
&= \{\mathbf{G}\,(y)\} \cdot (\{\mathbf{S}\,(C_1)\} \cap \{\mathbf{S}\,(C_2)\}) \\
&= \{\mathbf{G}\,(y)\} \cdot \{\mathbf{R}\,(C_1, \widehat{c_1 c_2})\}.
\end{aligned}
\tag{7}
$$

The above equation implies that the feasible movements of a grasped object with a 2F-2RR hand under the assumption of point contact with friction are the composition of a planar gliding displacement parallel to the xz-plane (two translations and one rotation about the normal to the plane) and a rotation about the axis defined by the contact points C_1 and C_2. Note that, as expected from the structural mobility of the closed kinematic chain of the hand–object system, the obtained finite displacement is a four-manifold.

C. Uncontrollable Displacements

The fifth (and final) step of the finite precision manipulation analysis is to determine if the feasible displacements of the grasped object can be controlled by the actuated joints of the robot hand. The minimum number of actuated joint axes for the hand–object system is given by the structural mobility M computed in the second step. Then, for determining if the resulting degrees of freedom of the grasped object can be controlled by the possible hand actuators, we just have to lock the joint axes affected by the actuation scheme when it is active, provided that this number is greater or equal than M, and repeat the four steps previously discussed. By locking, we mean equating all the controlled joint axes to $\{\mathbf{I}\}$, the identity displacement. If the resulting finite displacement after repeating the steps is the identity $\{\mathbf{I}\}$, then the selected scheme of actuation can control the different degrees of freedom because of the system becomes rigid. Otherwise, the result corresponds to the uncontrollable displacements of the grasped object.

In the case of the 2F-2RR hand with the model of point contact with friction, at least four joint axes have to be actuated since $M = 4$. This implies that both the proximal and distal joints of each finger in the hand have to be locked (i.e., $\{\mathbf{R}(A_1, y)\} = \{\mathbf{R}(A_2, y)\} = \{\mathbf{R}(B_1, y)\} = \{\mathbf{R}(B_2, y)\} = \{\mathbf{I}\}$). After repeating the steps one to four with these inputs, it can be verified that, in such a case, the obtained subset of $\{\mathbf{D}\}$ following the explained procedure is $\{\mathbf{R}(C_1, \widehat{c_1 c_2})\}$. In consequence, only three of the four degrees of freedom of the grasped object are controllable with the assumption of point contact with friction regardless of the friction conditions of the contacts. The rotation about the axis defined by the contact points C_1 and C_2 cannot be controlled by the actuators under the contact suppositions, thus depending on other external factors such as mass/disturbance forces.

IV. EXAMPLES

We present two additional examples of finite precision manipulation of robot hands. The first case details the manipulation analysis for a hand layout commonly found in commercial robot hands, assuming a point contact with friction model in all the fingertips. The second example focuses on the manipulation analysis of a four-fingered hand with revolute–revolute–revolute fingers manipulating an object with soft finger contacts.

A. Three-Fingered Hand With Universal–Revolute Fingers and Opposable Revolute–Revolute Thumb (3F-2UR1RR)

Fig. 4(top) shows a three-fingered hand with two universal–revolute (UR) fingers and an opposable revolute–revolute (RR) thumb, called herein the 3F-2UR1RR hand, grasping with its fingertips a general

object. The 3F-2UR1RR hand layout is used in some popular commercial robot hands such as the Schunk Hand [20] or the ReFlex Hand [5]. During tasks of precision manipulation, with the assumption of point contact with friction (step 1), the hand–object system of the 3F-2UR1RR hand is equivalent to a closed kinematic chain composed of eight links with two universal–revolute–spherical serial limbs and a revolute–revolute–spherical serial chain that connect the base of the robot hand to the grasped object. The mobility of this closed kinematic chain (eight links, nine joints in $\mathbb{E}^3$ with a total number of 17 DOF in the joints) is 5 (step 2).

According to the notation of Fig. 4(top), let us call finger 1, finger 2, and finger 3, the fingers with contact points C_1, C_2, and C_3, correspondingly. For the first finger, the proximal joint is a universal pair whose axes of rotation are determined by the unit vectors u_1 and w_1, that are parallel to the xy-plane and to the z-axis, respectively, and the meeting point of the axes, say A_1. This kinematic pair corresponds to a kinematic constraint that forms the submanifold $\{\mathbf{S}_2\,(A_1)\} = \{\mathbf{R}\,(A_1, z)\} \cdot \{\mathbf{R}\,(A_1, u_1)\}$, defined as the composition of two different subgroups of rotations whose axes meet at a single point. Taking into account that fingers 1 and 2 have the same configuration, and that finger 3 is equivalent to the fingers of the 2F-2RR hand, then, for the hand–object system of the 3F-2UR1RR hand, we get the graph of kinematic constraints (step 3) that is depicted in Fig. 4(bottom-a).

In order to reduce the graph of kinematic constraints (step 4), we initially apply serial reductions. Thus, for the case of nodes 1, 2, 3, and 6—related to the hand's first finger, we have (with $u_1 \parallel v_1$)

$$
\begin{aligned}
\mathcal{S}_1 &= \{\mathbf{S}_2\,(A_1)\} \cdot \{\mathbf{R}\,(B_1, v_1)\} \cdot \{\mathbf{S}\,(C_1)\} \\
&= \{\mathbf{R}\,(A_1, z)\} \cdot \{\mathbf{R}\,(A_1, u_1)\} \cdot \{\mathbf{R}\,(B_1, u_1)\} \cdot \{\mathbf{S}\,(C_1)\} \\
&= \{\mathbf{D}\}.
\end{aligned}
\tag{8}
$$

A list of some of the generators of the subgroup $\{\mathbf{D}\}$ ($\{\mathbf{D}\}$ is a subgroup of itself) can be found in [9, p. 22]. In the same way, for the case of nodes 1, 4, 5, and 6—related to finger 2, we obtain

$$
\begin{aligned}
\mathcal{S}_2 &= \{\mathbf{R}\,(A_2, z)\} \cdot \{\mathbf{R}\,(A_2, u_2)\} \cdot \{\mathbf{R}\,(B_2, u_2)\} \cdot \{\mathbf{S}\,(C_2)\} \\
&= \{\mathbf{D}\}.
\end{aligned}
\tag{9}
$$

Finally, for the third finger (nodes 1, 6, 7, and 8), we have

$$
\begin{aligned}
\mathcal{S}_3 &= \{\mathbf{R}\,(A_3, u_3)\} \cdot \{\mathbf{R}\,(B_3, v_3)\} \cdot \{\mathbf{S}\,(C_3)\} \\
&= \{\mathbf{R}\,(A_3, x)\} \cdot \{\mathbf{R}\,(B_3, x)\} \cdot \{\mathbf{R}\,(C_3, x)\} \cdot \{\mathbf{S}_2\,(C_3)\} \\
&= \{\mathbf{G}\,(x)\} \cdot \{\mathbf{S}_2\,(C_3)\}.
\end{aligned}
\tag{10}
$$

After the above reductions, we get a graph of kinematic constraints of two nodes and three edges [see Fig. 4(bottom-b)]. To obtain a graph with a single couple of kinematic constraints, we apply parallel reduction to, for instance, the kinematic constraints $\mathcal{S}_1$ and $\mathcal{S}_3$ [(8) and (10)], and $\mathcal{S}_2$ and $\mathcal{S}_3$ [(9) and (10)]. We can choose, in fact, any possible combinations of edges (e.g., $\mathcal{S}_1$ and $\mathcal{S}_2$, and $\mathcal{S}_2$ and $\mathcal{S}_3$). In any case, since $\lambda = 2$ in the original graph of kinematic constraints, up to three parallel reductions are needed to reduce the graph to two nodes and a single edge. Now, for $\mathcal{S}_1$ and $\mathcal{S}_3$, we have

$$
\begin{aligned}
\mathcal{P}_1 &= \mathcal{S}_1 \cap \mathcal{S}_3 = \mathcal{S}_3 \cap \mathcal{S}_1 \\
&= \{\mathbf{G}\,(x)\} \cdot \{\mathbf{S}_2\,(C_3)\} \cap \{\mathbf{D}\} \\
&= \{\mathbf{G}\,(x)\} \cdot \{\mathbf{S}_2\,(C_3)\}.
\end{aligned}
\tag{11}
$$

$\mathcal{P}_1$ is a five-manifold, as expected from the structural mobility of the closed kinematic chain associated with the kinematic constraints $\mathcal{S}_1$ and $\mathcal{S}_3$. Analogously, for $\mathcal{S}_2$ and $\mathcal{S}_3$, we get

$$
\begin{aligned}
\mathcal{P}_2 &= \mathcal{S}_2 \cap \mathcal{S}_3 = \mathcal{S}_3 \cap \mathcal{S}_2 \\
&= \{\mathbf{G}(x)\} \cdot \{\mathbf{S}_2(C_3)\} \cap \{\mathbf{D}\} \\
&= \{\mathbf{G}(x)\} \cdot \{\mathbf{S}_2(C_3)\}.
\end{aligned}
\tag{12}
$$

After the application of the two above parallel reductions, a graph of kinematic constraints of two nodes with two edges is obtained [see Fig. 4(bottom-c)]. Finally, for obtaining the subset of displacements of the grasped object, we apply a last parallel reduction to the constraints $\mathcal{P}_1$ and $\mathcal{P}_2$ [see Fig. 4(bottom-d-)]. Thus, we get

$$
\begin{aligned}
\mathcal{P}_3 &= \mathcal{P}_1 \cap \mathcal{P}_2 = \mathcal{S}_1 \cap \mathcal{S}_2 \cap \mathcal{S}_3 \\
&= \{\mathbf{G}(x)\} \cdot \{\mathbf{S}_2(C_3)\} \cap \{\mathbf{G}(x)\} \cdot \{\mathbf{S}_2(C_3)\} \\
&= \{\mathbf{G}(x)\} \cdot \{\mathbf{S}_2(C_3)\}.
\end{aligned}
\tag{13}
$$

The above equation implies that the feasible movements of a grasped object with a 3F-2UR1RR hand, under the assumption of point contact with friction, are the composition of a planar gliding displacement parallel to the yz-plane (two translations and one rotation about the normal to the plane) and two rotations about any two linearly independent axes, different to (C_3, x), that meet at point C_3. The obtained finite displacement is a five-manifold, as expected from the structural mobility of the closed kinematic chain of the hand–object system. Moreover, it can be verified that any selection of five actuated axes in the hand from the possible eight joints (considering the universal joints as two revolute joints that can be independently actuated), generates the identity displacement. Hence, there are not uncontrollable degrees of freedom in the hand–object system (step 5). This example was also discussed in [13] with equivalent results, but here we amend some of the steps in the deduction of (13).

B. Four-Fingered Hand With Revolute–Revolute–Revolute Fingers (4F-4RRR)

Fig. 5(left) shows a four-fingered hand with four revolute–revolute–revolute fingers (4F-4RRR) grasping, with its fingertips, a general object. During tasks of precision manipulation, assuming soft finger contacts in all the fingertips (step 1), the hand–object system of this hand is equivalent to a closed kinematic chain composed of 14 links with four revolute–revolute–revolute–universal serial limbs that connect the base of the robot hand to the grasped object. The mobility of this closed kinematic chain (14 links, 16 joints in $\mathbb{E}^3$ with a total number of 20 DOF in the joints) is 2 (step 2). The corresponding graph of kinematic constraints (step 3), according to the notation of Fig. 5(top), is depicted in Fig. 5(right-a).

Let us call finger 1, finger 2, finger 3, and finger 4, the fingers with contact points C_1, C_2, C_3, and C_4, correspondingly. Then, in order to reduce the graph of kinematic constraints (step 4), we initially apply serial reductions. For the case of the first finger (nodes 1, 2, 3, 4, and 14), we have (with $u_1 \parallel v_1 \parallel w_1$)

$$
\begin{aligned}
\mathcal{S}_1 &= \{\mathbf{R}(A_1, u_1)\} \cdot \{\mathbf{R}(B_1, u_1)\} \cdot \{\mathbf{R}(D_1, u_1)\} \\
&\quad \cdot \{\mathbf{S}_2(C_1)\} \\
&= \{\mathbf{G}(u_1)\} \cdot \{\mathbf{S}_2(C_1)\} \\
&= \{\mathbf{G}(u_1)\} \cdot \{\mathbf{R}(C_1, u_1)\} \cdot \{\mathbf{S}_2(C_1)\} \\
&= \{\mathbf{G}(u_1)\} \cdot \{\mathbf{S}(C_1)\}.
\end{aligned}
\tag{14}
$$

Similarly, for the case of fingers 2, 3, and 4, with $u_2 \parallel v_2 \parallel w_2$, $u_3 \parallel v_3 \parallel w_3$, $u_4 \parallel v_4 \parallel w_4$, $u_1 \parallel u_3$, and $u_2 \parallel u_4$, we obtain

$$
\mathcal{S}_2 = \{\mathbf{G}(u_2)\} \cdot \{\mathbf{S}(C_2)\}
\tag{15}
$$

$$
\mathcal{S}_3 = \{\mathbf{G}(u_1)\} \cdot \{\mathbf{S}(C_3)\}, \text{ and}
\tag{16}
$$

$$
\mathcal{S}_4 = \{\mathbf{G}(u_2)\} \cdot \{\mathbf{S}(C_4)\}
\tag{17}
$$

respectively.

After the above reductions, we get a graph of kinematic constraints of two nodes and four edges [see Fig. 5(right-b)]. To obtain a graph with a single couple of kinematic constraints, we apply parallel reduction to, for instance, the kinematic constraints $\mathcal{S}_1$ and $\mathcal{S}_3$ [(14) and (16)], and $\mathcal{S}_2$ and $\mathcal{S}_4$ [(15) and (17)]. For $\mathcal{S}_1$ and $\mathcal{S}_3$, we have

$$
\begin{aligned}
\mathcal{P}_1 &= \mathcal{S}_1 \cap \mathcal{S}_3 = \mathcal{S}_3 \cap \mathcal{S}_1 \\
&= \{\mathbf{G}(u_1)\} \cdot \{\mathbf{S}(C_1)\} \cap \{\mathbf{G}(u_1)\} \cdot \{\mathbf{S}(C_3)\} \\
&= \{\mathbf{G}(u_1)\} \cdot \{\mathbf{R}(C_1, \widehat{c_1 c_3})\}.
\end{aligned}
\tag{18}
$$

Correspondingly, for $\mathcal{S}_2$ and $\mathcal{S}_4$, we get

$$
\begin{aligned}
\mathcal{P}_2 &= \mathcal{S}_2 \cap \mathcal{S}_4 = \mathcal{S}_4 \cap \mathcal{S}_2 \\
&= \{\mathbf{G}(u_2)\} \cdot \{\mathbf{S}(C_2)\} \cap \{\mathbf{G}(u_2)\} \cdot \{\mathbf{S}(C_4)\} \\
&= \{\mathbf{G}(u_2)\} \cdot \{\mathbf{R}(C_2, \widehat{c_2 c_4})\}.
\end{aligned}
\tag{19}
$$

After the application of the above parallel reductions, a graph of kinematic constraints of two nodes with two edges is obtained [see Fig. 5(right-c)]. Finally, we apply a last parallel reduction to the constraints $\mathcal{P}_1$ and $\mathcal{P}_2$ [see Fig. 5(right-d)]. Thus, we obtain

$$
\begin{aligned}
\mathcal{P}_3 &= \mathcal{P}_1 \cap \mathcal{P}_2 \\
&= \{\mathbf{G}(u_1)\} \cdot \{\mathbf{R}(C_1, \widehat{c_1 c_3})\} \cap \{\mathbf{G}(u_2)\} \\
&\quad \cdot \{\mathbf{R}(C_2, \widehat{c_2 c_4})\} \\
&= \{\mathbf{T}(z)\} \cdot \{\mathbf{R}(C_1, \widehat{c_1 c_2})\}
\end{aligned}
\tag{20}
$$

since u_1 and $\widehat{c_1 c_3}$, and u_2 and $\widehat{c_2 c_4}$ are linearly independent vectors.

The above equation implies that the feasible movements of a grasped object with a 4F-4RRR hand, under the assumption of soft finger contacts, are the composition of a translational displacement along the z-axis and a rotation about the axis defined by the contact points C_1 and C_2. As expected from the structural mobility of the closed kinematic chain of the hand–object system, the obtained finite displacement is a two-manifold. It can be verified that any selection of two actuated axes in the hand from the possible 12 joints generates the identity displacement when the contacts are in general position. Hence, under these circumstances, there are not uncontrollable degrees of freedom in the hand–object system (step 5). However, if the contact points of fingers 1 and 3, and those of fingers 2 and 4, are at the same level respect to the palm, an uncontrollable displacement can be indeed identified.

1) Case of Uncontrollable Displacement: When contact points C_1 and C_3 are located at the same level respect to the palm of the robot hand, vectors u_2 and $\widehat{c_1 c_3}$ are parallel. In this case, (21) becomes

$$
\mathcal{P}_1^* = \{\mathbf{G}(u_1)\} \cdot \{\mathbf{R}(C_1, u_2)\}.
\tag{21}
$$

Likewise, for contact points C_2 and C_4 located at the same level ($u_1 \parallel \widehat{c_2 c_4}$), (19) becomes

$$
\mathcal{P}_2^* = \{\mathbf{G}(u_2)\} \cdot \{\mathbf{R}(C_2, u_1)\}.
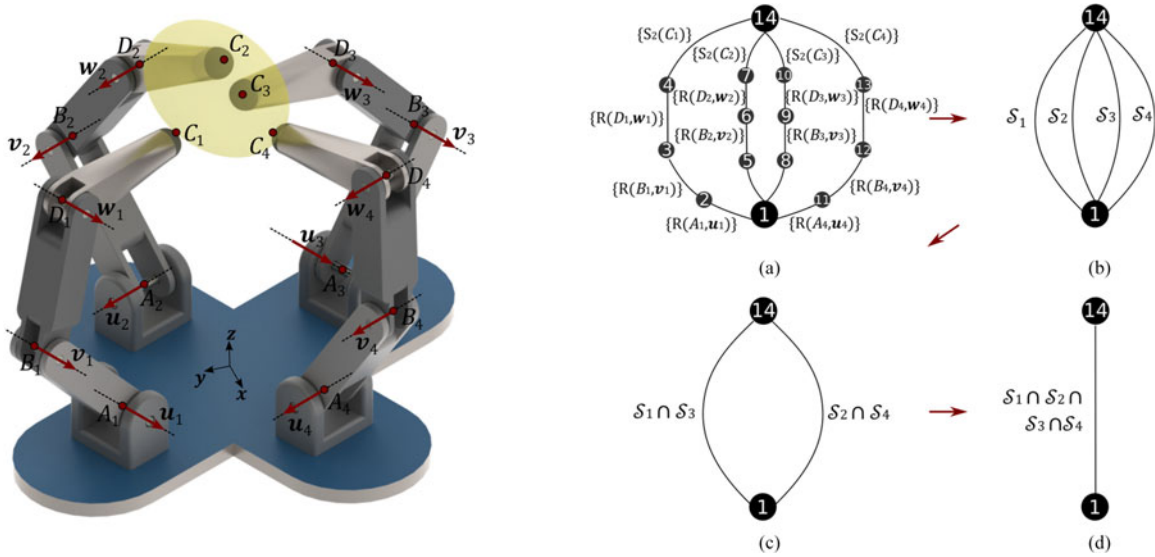\tag{22}
$$

Fig. 5. Left: A 4F-4RRR robot hand grasping an object with the notation used for its precision manipulation analysis with soft finger contacts. Right: The graph of kinematic constraints of the hand–object system for the 4F-4RRR hand (a) and its corresponding reduction (b, c, d).

Then, the parallel reduction of the kinematic constraints $\mathcal{P}_1^*$ and $\mathcal{P}_2^*$ that finally gives the feasible movements of the grasped object yields

$$
\begin{aligned}
\mathcal{P}_3^* &= \mathcal{P}_1^* \cap \mathcal{P}_2^* \\
&= \{\mathbf{G}(u_1)\} \cdot \{\mathbf{R}(C_1, u_2)\} \cap \{\mathbf{G}(u_2)\} \cdot \{\mathbf{R}(C_2, u_1)\} \\
&= \{\mathbf{T}(z)\} \cdot \{\mathbf{R}(C_1, u_2)\} \cdot \{\mathbf{R}(C_2, u_1)\}
\end{aligned}
\tag{23}
$$

since $u_1 \perp u_2$.

The above equation indicates that the resulting finite displacement of the grasped object is a three-manifold rather than a two-manifold, as expected from the structural mobility of the closed kinematic chain of the hand–object system. This implies that a contribution from $\varepsilon_1(\boldsymbol{\alpha})$ has been detected in the reduction process of the graph. In consequence, under the consideration of the contact locations, selections of two actuated axes in the hand from the possible 12 joints cannot control all the feasible displacements of the grasped object. For instance, if we just controlled the proximal joints of fingers 1 and 3, it results that the finite displacement of the object is $\{\mathbf{R}(C_1, u_2)\}$ instead of $\{\mathbf{I}\}$ as in the case of contacts in general position. In consequence, in such instances, the grasped object has a rotation about the axis defined by the contact point C_1 and the vector u_2 that is not controlled by the actuators but by external factors, such as mass/disturbance forces.

V. CONCLUSION

Precision manipulation can be considered the repositioning of a grasped object within the hand workspace without breaking or changing the assumed contact model. In this paper, we have presented a method based on the continuous group of displacements and the reduction of graphs of kinematic constraints to analyze the finite precision manipulation capabilities of a given robot hand. Finite manipulation refers to the information on the motion of the object that does not depend on its geometry or the particular dimensions of the fingers and the relations between the locations of the links composing them. The analysis allows determining the feasible movements to reposition any grasped object within the hand workspace as well as defining which of these possible displacements can actually be controlled by the hand actuators without depending on external factors to the hand.

The effects of a fingertip contacting a body in the presented analysis are modeled as kinematic chains, what permits using all standard contact categories of robotic manipulation (e.g., point contact with friction, soft finger) as well as other more complex contact models. The introduced precision manipulation analysis approach is general and can be applied to any finger/palm layout or subset of it. In terms of possible applications, the presented technique can be used, for instance, in early stages of robot hand and fingertip design to incorporate manipulation primitives needed to perform specific tasks. However, if a study of the topological properties of the resulting displacement manifolds is required, other techniques should be implemented.

REFERENCES

[1] I. M. Bullock, R. R. Ma, and A. M. Dollar, "A hand-centric classification of human and robot dexterous manipulation," *IEEE Trans. Haptics*, vol. 6, no. 2, pp. 129–144, Apr./Jun. 2013.

[2] A. Bicchi, "Hands for dexterous manipulation and robust grasping: a difficult road toward simplicity," *IEEE Trans. Robot. Autom.*, vol. 16, no. 6, pp. 652–662, Dec. 2000.

[3] M. Grebenstein *et al.*, "The hand of the DLR Hand Arm System: Designed for interaction," *Int. J. Robot. Res.*, vol. 31, pp. 1531–1555, 2012.

[4] K. Yamaguchi, Y. Hirata, and K. Kosuge, "Development of robot hand with suction mechanism for robust and dexterous grasping," in *Proc. IEEE/RSJ Int. Conf. Intell. Robot. Syst.*, 2013, pp. 5500–5505.

[5] L. U. Odhner *et al.*, "A compliant, underactuated hand for robust manipulation," *Int. J. Robot. Res.*, vol. 33, pp. 736–752, 2014.

[6] P. Michelman, "Precision object manipulation with a multifingered robot hand," *IEEE Trans. Robot. Autom.*, vol. 14, no. 1, pp. 105–113, Feb. 1998.

[7] T. Hasegawa, K. Murakami, and T. Matsuoka, "Grasp planning for precision manipulation by multifingered robotic hand," in *Proc. IEEE Int. Conf. Syst., Man, Cybern.*, 1999, vol. 6, pp. 762–767.

[8] J. M. Hervé, "Analyse structurelle des mécanismes par groupe des déplacements," *Mechanism Mach. Theory*, vol. 13, pp. 437–450, 1978.

[9] J.-P. Merlet, *Parallel Robots*, vol. 128. Berlin, Germany: Springer-Verlag, 2006.

[10] L. Qinchuan and J. M. Herve, "Type synthesis of 3-DOF RPR-equivalent parallel mechanisms," *IEEE Trans. Robot.*, vol. 30, no. 6, pp. 1333–1343, Dec. 2014.

[11] X. Kong and C. Gosselin, *Type Synthesis of Parallel Mechanisms*. London, U.K.: Springer-Verlag, 2007.

[12] J. M. Hervé, "The Lie group of rigid body displacements, a fundamental tool for mechanism design," *Mechanism Mach. Theory*, vol. 34, pp. 719–730, 1999.

[13] N. Rojas and A. M. Dollar, "Characterization of the precision manipulation capabilities of robot hands via the continuous group of displacements," in *Proc. IEEE/RSJ Int. Conf. Intell. Robots Syst.*, Chicago, IL, USA, Sep. 14–18, 2014.

[14] N. Rojas and A. M. Dollar, "Classification and kinematic equivalents of contact types for the precision manipulation analysis of multifingered robot hands," *ASME J. Mechanisms Robot.*, vol. 8, no. 4, 2016, Art. no. 041014.

[15] C. R. Tischler, A. E. Samuel, and K. H. Hunt, "Kinematic chains for robot hands—II: Kinematic constraints, classification, connectivity, and actuation," *Mechanism Mach. Theory*, vol. 30, pp. 1217–1239, 1995.

[16] J. K. Salisbury and B. Roth, "Kinematic and force analysis of articulated mechanical hands," *J. Mechanisms Transmiss. Autom. Des.*, vol. 105, pp. 35–41, 1983.

[17] E. Rimon and J. W. Burdick, "Mobility of bodies in contact—I: A 2nd-order mobility index for multiple-finger grasps," *IEEE Trans. Robot. Autom.*, vol. 14, no. 5, pp. 696–708, Oct. 1998.

[18] C. W. Wampler, J. D. Hauenstein, and A. J. Sommese, "Mechanism mobility and a local dimension test," *Mechanism Mach. Theory*, vol. 46, pp. 1193–1206, 2011.

[19] A. Müller, "Generic mobility of rigid body mechanisms," *Mechanism Mach. Theory*, vol. 44, pp. 1240–1255, 2009.

[20] Schunk, SDH Servo-Electric 3-Finger Gripping Hand. (2012). [Online]. Available: http://mobile.schunk-microsite.com/en/produkte/products/sdh-servo-electric-3-finger-gripping-hand.html